Journal of Geodetic Science
• 2(3) • 2012 • 224-233 DOI: 10.2478/v10156-011-0043-6 •

Detection of main tidal frequencies using least squares harmonic estimation method

Research Article

R. Mousavian * and M. Mashhadi Hossainali

Department of Geodesy and Geomatics Engineering, K. N. Toosi University of Technology, Tehran, Iran

Abstract:
In this paper the efficiency of the method of Least Squares Harmonic Estimation (LS-HE) for detecting the main tidal frequencies is investigated. Using this method, the tidal spectrum of the sea level data is evaluated at two tidal stations: Bandar Abbas in south of Iran and Workington on the eastern coast of the UK. The amplitudes of the tidal constituents at these two tidal stations are not the same. Moreover, in contrary to the Workington station, the Bandar Abbas tidal record is not an equispaced time series. Therefore, the analysis of the hourly tidal observations in Bandar Abbas and Workington can provide a reasonable insight into the efficiency of this method for analyzing the frequency content of tidal time series. Furthermore, applying the method of Fourier transform to the Workington tidal record provides an independent source of information for evaluating the tidal spectrum proposed by the LS-HE method. According to the obtained results, the spectrums of these two tidal records contain the components with the maximum amplitudes among the expected ones in this time span and some new frequencies in the list of known constituents. In addition, in terms of frequencies with maximum amplitude; the power spectrums derived from two aforementioned methods are the same. These results demonstrate the ability of LS-HE for identifying the frequencies with maximum amplitude in both tidal records.

Keywords:
Least squares harmonic estimation • spectral analysis • tidal frequencies

Received 10-07-2012; accepted 27-09-2012

1. Introduction

Analyzing the frequency content of the coordinate time series in an active tectonic region is now an accepted method for understanding the kinematics of deformation (Ghil and Taricco 1997). The applied methods normally assume the input as a periodic time series. The efficiency of these methods can be practically evaluated through their application to a periodic time series like tidal records whose frequency content has been already established. Least-Squares Harmonic Estimation (LS-HE) is one of the existing methods that has been recently developed by Amiri-Simkooei (2007). This paper intends to investigate the efficiency of LS-HE in detecting the frequency content of a periodic time series. The ocean tide has been used for this purpose.

The ocean tide is the periodic variation of sea level due to the tidal acceleration produced by celestial bodies (Epler 2010). For a spherically symmetric Earth the tidal acceleration is the difference between the Earth orbital acceleration which is caused by the attraction of the celestial body at the Earth's center of mass and that at the point of observation (Agnew 2007). In potential theory the tidal acceleration is expressed in terms of tidal potential.
If M is the mass of the external body, the gravitational potential, V, from it at the origin O using the cosine rule from trigonometry, is computed from the following equation (Agnew 2007, Vanicek 1987):

$$V_t(O) = \frac{GM}{R}\frac{1}{[1+(a/R)^2-2(a/R)\cos\alpha]^{1/2}} - \left[\frac{GM}{R} - \frac{GM}{R^2}a\cos\alpha\right] \quad (1)$$

The variables are as shown in Fig. 1: a is the distance of O from C, ρ the distance from O to M, and α the angular distance between

*E-mail: r_mousavian@yahoo.com

VERSITA

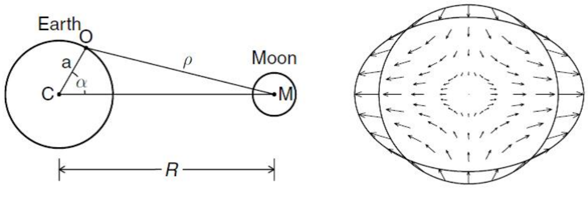

Figure 1. Tidal forcing. On the left is the geometry of the problem for computing the tidal force at a point O on the Earth, given an external body M. The right plot shows the field of forces (accelerations) for the actual Earth–Moon separation (Agnew, 2007).

O and the sub-body point of M. The first and the second terms in Eq. (1) are the Moon's gravitational and orbital potentials at point O respectively. Using the Legendre generating-function (in the first term) and the Legendre functions of degree zero and one (in the second term) yields

$$V_t(O) = \frac{GM}{R}\sum_{n=0}^{\infty}\left(\frac{a}{R}\right)^n p_n(\cos(\alpha)) - \frac{GM}{R}\sum_{n=0}^{1}\left(\frac{a}{R}\right)^n p_n(\cos(\alpha)) = \frac{GM}{R}\sum_{n=2}^{\infty}\left(\frac{a}{R}\right)^n p_n(\cos(\alpha)) \tag{2}$$

Variations of the parameters R and α in Eq. (2) show that the tidal potentials generated by the celestial bodies are not the same. Moreover, the tidal potential is not constant throughout the Earth and includes a number of periodic frequencies (Epler 2010). Extensive computations of the tidal potential and its harmonic decomposition has been done in order to achieve more precision in analyzing the tidal data [for example Darwin 1907, Doodson 1921, Cartwright and Tayler 1971, Kudryavtsev 2004]. Among those who have worked on the tide, results given by Kudryavtsev provide the spectrum of the tide in more details (Kudryavtsev 2004). According to this research, 27000 frequencies are required for accurate modeling of the tidal signal whose amplitudes are mostly small. The tidal frequencies can be generally classified into four groups: (a) semi diurnal, (b) diurnal, (c) long period and (d) short period ones. Tables 1 through 4 provide some of these frequencies based on the naming system proposed by Darwin (Darwin 1907, Wahr 1995; House, 1995). Figure 2 compares the amplitudes of the diurnal and semi-diurnal components computed by Hartman and Wenzel (1995). In this figure Darwin's symbols are used for the larger harmonics. The larger amplitude of the semidiurnal component of the moon (M_2) is remarkable in these results.

In this paper, the efficiency of the Least Squares Harmonic Estimation (LS-HE) for detecting the main frequencies in the tidal spectrum is analyzed. The next section of this paper discusses the theoretical background of this method. Using this method, the tidal spectrum of the sea level data is evaluated at two tidal stations: Bandar Abbas in south of Iran and Workington on the eastern coast of the UK. In contrary to Workington station, the Bandar Abbas tidal record is not an equidispace time series. Therefore, the analysis of the hourly tidal observations in Bandar Abbas and Workington can provide a reasonable insight into the efficiency of this method for analyzing the frequency content of tidal time series. Moreover, applying the method of Fourier transform to the Workington tidal record provides an independent source of information for evaluating the tidal spectrum proposed by the method of LS-HE. Section 3 provides the corresponding numerical results. Simulated time series have been used for validating the computer codes which have

Table 1. Diurnal components of tide (Wahr 1995,House 1995).

No.	Tidal component	Period(hour)
1	Lunar diurnal K_1	23.9344
2	Lunar diurnal O_1	25.8193
3	Lunar diurnal OO_1	22.3060
4	Solar diurnal S_1	24
5	M_1	24.8412
6	J_1	23.09848
7	ρ	26.7230
8	Q_1	26.8683
9	$2Q_1$	28.0062
10	Solar diurnal P_1	24.06588

Table 2. Semidiurnal component of tide (Wahr 1995,House 1995)

No.	Tidal component	Period (hour)
1	Principal lunar semidiurnal M_2	12.4206
2	Principal solar semidiurnal S_2	12
3	N_2	12.658
4	υ_2	12.626
5	MU_2	12.871
6	$2N_2$	12.905
7	λ_2	12.221
8	T_2	12.016
9	R_2	11.983
10	$2SM_2$	11.606
11	L_2	12.191
12	K_2	11.967

Table 3. Shallow water components or short period components of tide (Wahr 1995, House 1995).

No.	Tidal component	Period (hour)
1	M_4	6.021030
2	M_6	4.1404
3	MK_3	8.1771
4	S_4	6
5	MN_4	6.26917
6	S_6	4
7	M_3	8.2863
8	$2MK_3$	8.3863
9	M_8	3.10515
10	MS_4	6.10333

Table 4. Long period components of tide (Wahr 1995, House 1995).

No.	Tidal component	Period (hour)
1	Lunar monthly M_m	661.3111
2	Solar semiannual M_{Sa}	4383.0763
3	Solar annual Sa	8766.15265
4	M_{Sf}	354.36706

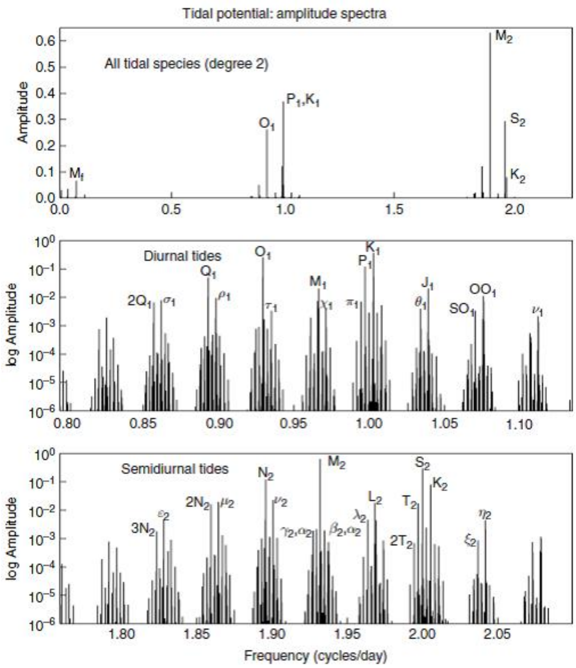

Figure 2. Normalized amplitudes of the detected frequencies in tidal spectrum (Hartman and Wenzel, 1995).

been developed for this purpose. This section of the paper also reports on the corresponding results.

2. Least Squares Harmonic Estimation (LS-HE)

The least squares harmonic estimation (LS-HE) is a method which was first introduced and applied to GPS position time series by Amiri-Simkooei (see Amiri-Simkooei 2007 and Amiri-Simkooei et al. 2007). The method is based on the application of harmonic functions for modeling the periodic constituents of a phenomenon. As a generalization of the Fourier spectral analysis, the method is neither limited to evenly spaced data nor to integer frequencies (Amiri-Simkooei and Asgari 2012). The method is actually based on the Least Squares Spectral Analysis (LSSA) developed by Vanicek 1996 even when an initial design matrix is present in the model and the covariance matrix, in general, is not a scaled identity matrix. Amiri-Simkooei and Tiberius (2007), Amiri-Simkooei and Asgari (2012) provide some examples for the application for this method. This paper is the first attempt for the application of this method to the analysis of tidal data.

The functional model of a periodic time series $y^T = [y_1, y_2, ..., y_m]$, which is defined on R^m, is in general given by:

$$\mathbf{y} = \mathbf{y_0} + r\mathbf{t} + \sum_{k=1}^{q} a_k \cos(\omega_k \mathbf{t}) + b_k \sin(\omega_k \mathbf{t}) \tag{3a}$$

Or in matrix notation:

$$\mathbf{y} = \mathbf{Ax} + \sum_{k=1}^{q} \mathbf{A_k x_k} \tag{3b}$$

In these equations, $\mathbf{y_0}$ is the zero frequency component of the time series, r is linear rate, a_k and b_k are amplitudes of sine and cosine components corresponding to the frequency ω_k and t_i for $i = 1, 2, ..., m$ are observation epochs. The two column matrix $\mathbf{A}$ contains the coefficients of the linear regression part of the model, whereas the two column matrices $\mathbf{A_k}$ are constructed by the corresponding coefficients for the trigonometric components of frequencies ω_k:

$$\mathbf{A_k} = \begin{bmatrix} \cos\omega_k t_1 & \sin\omega_k t_1 \\ \cos\omega_k t_2 & \sin\omega_k t_2 \\ \vdots & \vdots \\ \cos\omega_k t_m & \sin\omega_k t_m \end{bmatrix} \;;\; \mathbf{x} = \begin{bmatrix} y_0 \\ r \end{bmatrix} \;;\; \mathbf{x_k} = \begin{bmatrix} a_k \\ b_k \end{bmatrix} \tag{4}$$

When in Eq. (3) ω_k is known, linear least-squares is used for solving the problem. Least Squares Harmonic Estimation has been proposed for finding the unknown parameters in Eq. (3) when the unknown parameters are both ω_k and the coefficients a_k and b_k.
To apply the Least Squares Harmonic Estimation, the unknown frequencies $\omega_1, \omega_2, ...\omega_q$ are firstly determined. This is done recursively through q statistical hypotheses below in which i runs from 1 to q (Amiri-Simkooei, 2007):

$$\begin{cases} H_\circ : \;\; \mathbf{y} = \mathbf{Ax} + \sum_{k=1}^{i-1} \mathbf{A_k x_k} \\ H_a \;: \mathbf{y} = \mathbf{Ax} + \sum_{k=1}^{i} \mathbf{A_k x_k} \end{cases} \tag{5}$$

Evaluation of this hypothesis test consists of the two steps (Amiri-Simkooei, 2007): (a) solving the following minimization problem in order to detect the existing frequency ω_i

$$\omega_i = \arg\min_{\omega_j} \left\| \mathbf{P}_{[\overline{\mathbf{A}}\,\mathbf{A_j}]}^{\perp} \mathbf{y} \right\|^2_{\mathbf{Q_y}^{-1}} = \arg\min_{\omega_j} \left\| \hat{\mathbf{e}}_\mathbf{a} \right\|^2_{\mathbf{Q_y}^{-1}} \tag{6}$$

where $\|.\|^2_{\mathbf{Q_y}^{-1}} = (.)^T \mathbf{Q_y}^{-1} (.)$, $\overline{\mathbf{A}} = [\mathbf{A}, \mathbf{A_1}, \ldots, \mathbf{A_{i-1}}]$, $\mathbf{Q_y}$ is the variance-covariance matrix of observation and $\hat{\mathbf{e}}_\mathbf{a}$ is the least squares residuals under the alternative hypothesis. Sub-matrices $\mathrm{A_i}$ of matrix $\overline{\mathrm{A}}$ have the same structure as $\mathrm{A_k}$ given in Eq. (3) and are constructed using the frequencies which have been detected through previous evaluations of the statistical hypothesis 5. The matrix $\mathrm{A_j}$ has the same structure as $\mathrm{A_k}$ and is constructed using the frequency of interest. The minimization problem above is equivalent to the following maximization problem (Amiri-Simkooei 2007, Teunissen 2000a):

$$\omega_i = \arg\max_{\omega_j} \left\| \mathrm{P}_{\overline{\mathrm{A}}_j} \mathbf{y} \right\|^2_{\mathrm{Q_y}^{-1}} ; \quad \overline{\mathrm{A}}_j = \mathrm{P}^{\perp}_{\overline{\mathrm{A}}} \mathrm{A_j} \tag{7a}$$

$$\mathrm{P}^{\perp}_{\overline{\mathrm{A}}} = \mathrm{I} - \overline{\mathrm{A}}(\overline{\mathrm{A}}^{\mathrm{T}} \mathrm{Q_y}^{-1} \overline{\mathrm{A}})^{-1} \overline{\mathrm{A}}^{\mathrm{T}} \mathrm{Q_y}^{-1} \tag{7b}$$

$$\mathrm{P}_{\overline{\mathrm{A}}_j} = \overline{\mathrm{A}}_j (\overline{\mathrm{A}}_j^{\mathrm{T}} \mathrm{Q_y^{-1}} \overline{\mathrm{A}}_j)^{-1} \overline{\mathrm{A}}_j^{\mathrm{T}} \mathrm{Q_y^{-1}} \tag{7c}$$

Eq. (7a) can be re-written in following form in which $\hat{\mathrm{e}}_\circ = P^{\perp}_{\overline{A}} y$ is the least squares residuals under null hypothesis:

$$\omega_i = \arg\max_{\omega_j} \; \hat{\mathrm{e}}_0^{\mathrm{T}} \mathrm{Q_y^{-1}} \mathrm{A_j} (\mathrm{A_j^T} \mathrm{Q_y^{-1}} \mathrm{P}^{\perp}_{\overline{\mathrm{A}}} \mathrm{A_j})^{-1} \mathrm{A_j^T} \mathrm{Q_y^{-1}} \hat{\mathrm{e}}_0 \tag{8}$$

The analytical solution of the optimization problem given by Eq. (8) is complicated. Therefore, numerical methods are preferred to solve the problem. For this purpose, the power spectrum of the time series is produced using the spectral values of different frequencies. The spectral value of a frequency ω_j is computed by $\left\| \mathrm{P}_{\overline{\mathrm{A}}_j} \mathbf{y} \right\|^2_{\mathrm{Q_y}^{-1}}$. The continuous diagram in which the spectral values are plotted against their corresponding frequencies constructs the power spectrum of the time series. Consecutive frequencies with maximal spectral values are used for constructing the matrices A_i.
(b) The hypothesis test 5 is then evaluated using $\mathrm{Q_y} = \sigma^2 \mathrm{I}$ in which the a-priori variance of unit weight σ^2 is unknown. The following statistic is used for this purpose (see Teunissen et al. 2005, Amiri-Simkooei 2007):

$$T_2 = \frac{\left\| \mathrm{P}_{\overline{\mathrm{A}}_i} \mathbf{y} \right\|^2_{\mathrm{Q_y}^{-1}}}{2\hat{\sigma}_a^2} = \frac{\hat{\mathrm{e}}_0^{\mathrm{T}} \mathrm{A_i} (\mathrm{A_i^T} \mathrm{P}^{\perp}_{\overline{\mathrm{A}}} \mathrm{A_i})^{-1} \mathrm{A_i^T} \hat{\mathrm{e}}_0}{2\hat{\sigma}_a^2} \tag{9}$$

In Eq. (9), $\overline{\mathrm{A_i}} = \mathrm{P}^{\perp}_{\overline{\mathrm{A}}} \mathrm{A_i}$ and $\hat{\sigma}_a^2$ is the a-posteriori variance under alternative hypothesis which is computed by the following equation:

$$\hat{\sigma}_a^2 = \frac{\hat{\mathrm{e}}_a^{\mathrm{T}} \mathrm{Q_y^{-1}} \hat{\mathrm{e}}_a}{df} \tag{10}$$

In this equation: df is the degree of freedom under the alternative hypothesis of the statistical test 5. The distribution of the statistic 9 is central Fisher with 2 and $m - n - 2i$ degrees of freedom, that is:

$$T_2 \approx F(2, m - n - 2i) \tag{11}$$

A frequency whose statistic satisfies the inequality $T_2 > \xi_{F(2,m-n-2i)}$, where $\xi_{F(2,m-n-2i)}$ is the corresponding critical value of the central Fisher distribution, is taken as an acceptable frequency.
If σ were known, the applied statistic T_2 and the distribution function would change. In this case, the test statistic has a central chi-square distribution with two degrees of freedom (Amiri-Simkooei and Asgari 2012), that is:

$$T_2 \approx \chi^2(2, 0) \tag{12}$$

The computational step is evaluated using the following recursive relation (Amiri-Simkooei and Tiberius 2007):

$$T_{j+1} = T_j(1 + \alpha T_j / T), j = 1, 2, ... \tag{13}$$

The iteration starts from the Nyquist frequency $\omega_1 = \frac{2\pi}{T_1}$ and covers the total observation time span (T_j). T_1 is twice as large as the sampling time span. Reducing the coefficient α in Eq. (13) increases the number of frequencies to be analyzed.
After detecting the effective constituents in the desired time series, the remaining unknown parameters of the functional model, including the zero frequency component $\mathbf{y}_0$, linear rate r and amplitudes of the frequencies, are determined using the least squares estimation technique. According to the least squares method, the unknown parameters in functional relation $\mathbf{y} = \mathrm{Ax} + \mathrm{v}$ and variance-covariance matrix of the unknown parameters in this model are computed from following equations:

$$\hat{\mathrm{x}} = (\mathrm{A^T} \mathrm{Q_y^{-1}} \mathrm{A})^{-1} \mathrm{A^T} \mathrm{Q_y^{-1}} \mathbf{y} \tag{14}$$

$$\mathrm{Q}_{\hat{\mathrm{x}}} = (\mathrm{A^T} \mathrm{Q_y^{-1}} \mathrm{A})^{-1} \tag{15}$$

3. Numerical results

The hourly time series of two tidal stations Bandar Abbas and Workington from the tide gauge networks of Iran and UK are selected for this research, respectively. The lengths of the two time series have been limited to one year.
Figure 3 demonstrates the geographical position of the two aforementioned stations. In contrary to the station in Iran, the Workington tidal record is an equispaced time series. This makes it possible to compare the main tidal constituents of this station obtained from LS-HE and the Fourier transform. This can be a cross check for the efficiency of Least Squares Harmonic Estimation in detecting the existing constituents of a periodic time series.
To check the computer codes which have been developed in this research as well as the efficiency of LS-HE in detecting the complete spectrum of a periodic signal, simulated data sets have also been analyzed.

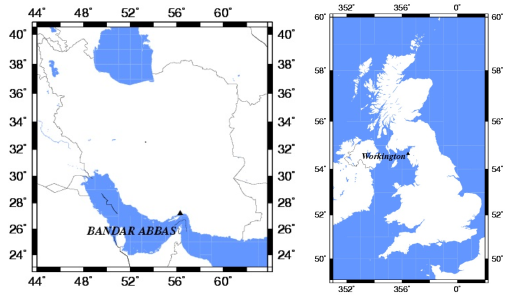

(a) (b)

Figure 3. Geogarphical position of the tidal stations: (a) Bandar Abbas, (b) Workington.

3.1. Analysis of simulated data sets

To simplify the procedure of checking the developed computer codes, two time series that only contain white noise are simulated. A set of known frequencies with pre-defined amplitudes are used for this purpose.

Table 5. Characteristics of the frequencies in the second simulated time series.

No.	Angular frequency (degrees)	Period (sampling rate)	Amplitude of frequency
1	30	12	2
2	40	9	1
3	120	3	1
4	20	18	0.44
5	54	6.6	0.37
6	88	4	1

The first time series includes the three angular frequencies: 30, 40 and 120 degrees which are equivalent to 12, 9 and 3 sampling rate. Similar amplitudes are used for these constituents in simulating the time series. In contrary to the first series, the amplitudes of the constituents in the second time series are not the same. Moreover, the second series includes six frequencies. The corresponding details of this series are given in Table 5. The data length in both of the two time series is 400 sampling rate.

Figure 4 and Fig. 5 show the power spectrums of the first and the second time series above. In these figures, the horizontal axes are the angular frequencies (in degrees) and the vertical axes illustrate the corresponding power spectrum for every frequency. Maximum power spectra for the first series exactly occur at the expected frequencies 3, 9 and 12. Moreover, using the confidence level of 99 percent, the significance of these frequencies is approved by the method of LS-HE. In contrary to the first series, maximum power spectra in the second one occur in only four frequencies of the six mentioned above (see Fig. 5). Using a similar confidence level, the statistical test in LS-HE only confirms the existence of these frequencies in the time series. It is interesting to note that the four detected frequencies are those whose amplitudes are much larger than the others (see Table 5) and therefore have a greater contribution in reconstructing the signal. The simulation results given above illustrate that the method of LS-HE is sensitive to the amplitudes of the frequencies which construct a periodic signal.

Although the dependency of LS-HE to the length of data is clear via the degree of freedom used in the statistic of its hypothesis test, the contribution of the data length in the efficiency of this method for detecting the frequencies with smaller power spectra as compared to the other frequencies is also analyzed. For this purpose, the length of data in the simulated second time series has been

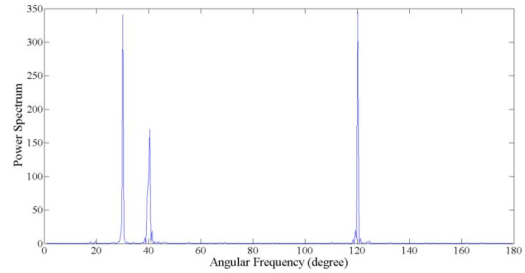

Figure 4. The power spectrum of the simulated time series one.

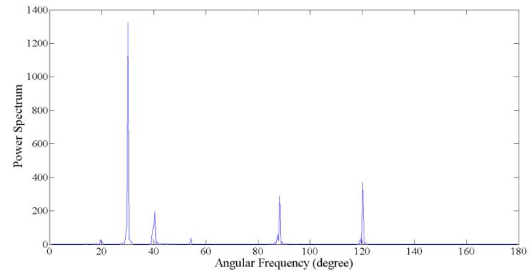

Figure 5. The power spectrum of the simulated time series two.

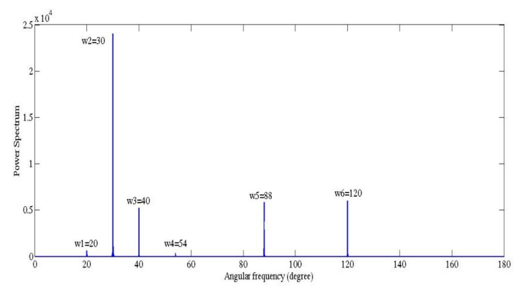

Figure 6. The power spectrum of the simulated time series contains 6000 sampling rate.

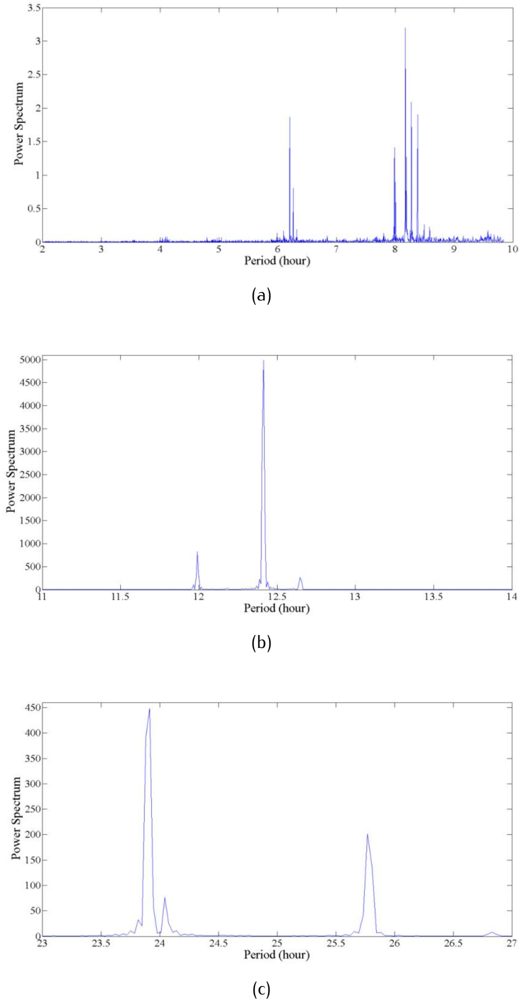

Figure 7. Power spectrum of the Bandar Abbas tidal record constructed for different time intervals: (a) short period components, (b) semidiurnal components, (c) diurnal components.

recursively increased from 400 to 6000 sampling rate. As a result, all of the 6 frequencies are detected. This result demonstrates the significant role of the length of data in accurate reconstruction of the functional model for a periodic time series through detecting its frequencies. Figure 6 illustrates the power spectrum of this time series. Horizontal and vertical axes in this figure are the same as those in Fig. 4 and Fig. 5.

3.2. Analysis of Bandar Abbas tidal records

To investigate the tidal constituents of the Bandar Abbas tidal records, the power spectrum of this time series is firstly constructed using the method discussed above. The corresponding parts for the short period, diurnal and semidiurnal tidal components of the constructed spectrum are shown in Fig. 7. The horizontal and vertical axes of this figure are time span or period and the power spectra for every frequency respectively.

Table 6. Detected frequencies of sea level data for Bandar Abbas station using LS-HE.

No.	Equivalent tidal constituent	Amplitude of components	Period of detected components (in hours)
1	M_2	1.075	12.423
2	S_2	0.412	11.998
3	K_1	0.314	23.946
4	N_2	0.248	12.655
5	H_1	0.0134	12.396
6	O_1	0.2087	25.808
7		0.0341	12.4492
8		0.082	11.974
9		0.0075	12.379
10	P_1	0.130	24.077
11		0.29	12.467
12		0.0189	12.024
13		0.0127	12.484
14	L_2	0.061	12.19

As it is expected, the power spectra of the semidiurnal components are much larger than the others (compare Fig. 7b to Fig. 7a and Fig. 7c). The small spectral values for the short period components illustrate their small contribution in constructing the signal as compared to the other components. Table 6 provides the constituents whose frequencies have been approved by the LS-HE method. The adopted confidence level is 99 percent.

The last column of this table gives the equivalent tidal constituents based on Darwin's naming system. According to the Rayleigh criterion (Abolghasem 1994) and research made by others, for example see (Epler 2010, Darwin 1907, Doodson 1921, Foreman 1977), many of the expected frequencies are not seen in this table (see appendix A for further details). Referring to appendix A, the constituents given in Table 6 are the components with larger amplitudes among the others. Moreover, some constituents are seen in Table 6 which have no equivalent name in the Darwin's naming system. Therefore, they have not been given any name in this table.

3.3. Analysis of Workington tidal records

The power spectrum of the Workington equispaced tidal time series has been estimated using both the LS-HE and Fourier Transform methods. The probability for the commitment of the type I error has been taken as 1% again. The accepted frequencies in the statistical test of LS-HE and their estimated amplitudes are given in Table 7. Again the last column of the table gives the equivalent tidal constituents based on Darwin's naming system. The results of this table in comparison with appendix A, illustrates that with a limited time series of tidal data the detection of tidal frequencies using the method of LS-HE is restricted to the tidal constituents whose amplitudes are large. In this case, similar to Bandar Abbas station

Table 7. Detected frequencies in sea level data of Workington station using LS-HE method.

No.	Equivalent tidal component	Amplitude of the component	Period of the detected components (in hours)
1	M_2	2.483	12.424
2	S_2	0.829	11.999
3	N_2	0.505	12.655
4	K_2	0.233	11.974
5	MKS_2	0.0184	12.38
6		0.066	12.468
7		0.042	12.486
8	T_2	0.0264	12.016
9	υ_2	0.1078	12.626
10		0.031	12.503
11		0.022	12.345
12	L_2	0.129	12.19
13	O_1	0.132	25.819
14		0.026	12.52
15	K_1	0.125	23.94
16	MN_4	0.121	6.211
17		0.016	12.68

there are some constituents which have no equivalent name in the Darwin's naming system. These constituents are seen in Table 7.

The computed power spectrum has been illustrated in Fig. 8 to Fig. 11. The LS-HE method has been used for this purpose. The horizontal and vertical axes in these figures are similar to those in Fig. 7. Figure 8 demonstrates short period components corresponding to shallow water effects: Figure 8a illustrates the components whose frequencies range from 3 to 4.5 hours, Figure 8b illustrates the components whose frequencies range from 6 to 7 hours and finally Fig. 8c illustrates the components whose frequencies range from 8 to 9 hours. As it is seen in these figures, the power spectrum of the constituent whose frequency is 6.21 hours is the largest compared to the others. This constituent is the only shallow water component which is approved by the LS-HE method. Figure 9 illustrates the semidiurnal components in the tidal power spectrum of the desired time series. As is expected, the power spectra of the semidiurnal components are much larger than the other constituents.

The power spectrum for the detected diurnal components of the desired time series is shown in Fig. 10. Again as is expected, the comparison of this figure with former ones illustrates that the power spectrum of the diurnal components are larger than those of the short period constituents and are much smaller than the power spectrum of the main semidiurnal components such as M_2.

Figure 11 illustrates the power spectrum for frequencies in the range of long period components. Peaks around the long period components such as 14 days can be seen in this figure. Nevertheless, the LS-HE method does not approve any constituent with a frequency in the long period range (see Table 4 and Table 7). As is expected again, the comparison of this figure with the former ones illustrates that the power spectrum of the long period components are smaller than those of the other constituents which have been already confirmed by the method. To check the impact of data length on the detected frequencies, the length of the Workington tidal time series has been gradually increased to 19 years. More expected frequencies are detected as the length of the data set is increased.

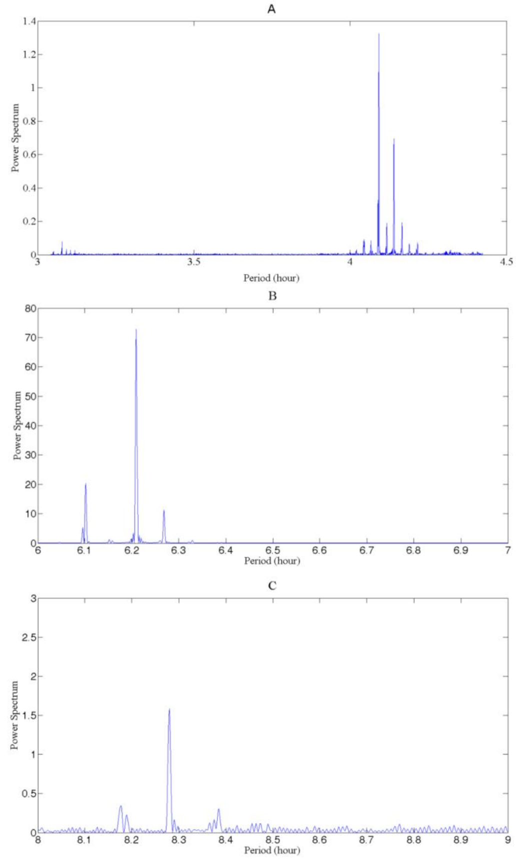

Figure 8. Obtained power spectrum from LS-HE method, indicative of short period components in Workington station's tidal spectrum. a) in range of 4 – 4.5 hours. b) in range of 6 – 7 hours. c) in range of 8 – 9 hours.

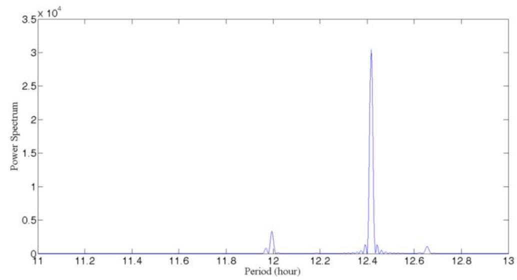

Figure 9. Obtained power spectrum from LS-HE method in range of semidiurnal components of tidal power spectrum

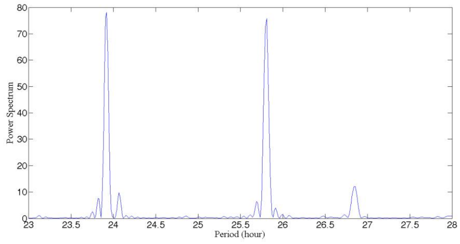

Figure 10. Obtained power spectrum from LS-HE method in range of diurnal components of tidal power spectrum

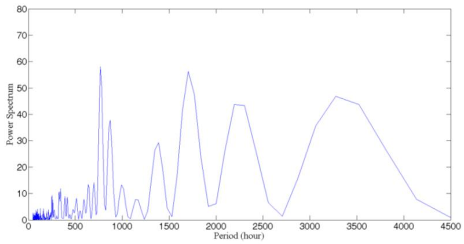

Figure 11. Obtained power spectrum from LS-HE method in range of long period components of tidal power spectrum

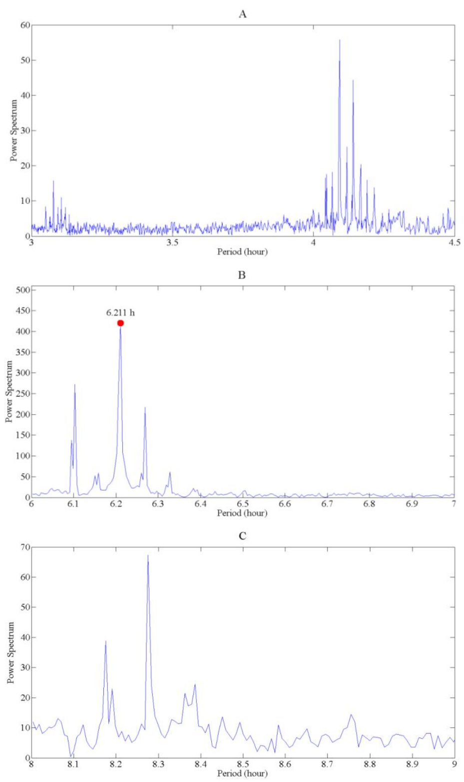

Figure 12. The power spectrum obtained from the method of Fourier Transform-short period components: (a) in range of 4 – 4.5 hours (b) in range of 6 – 7 hours, (c) in range of 8 – 9 hours.

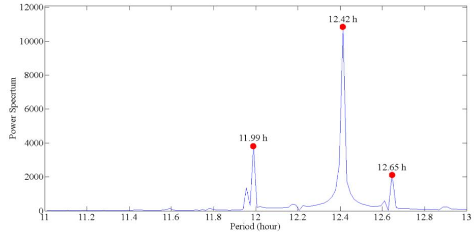

Figure 13. Power spectrum obtained from Fourier Transform - semidiurnal components.

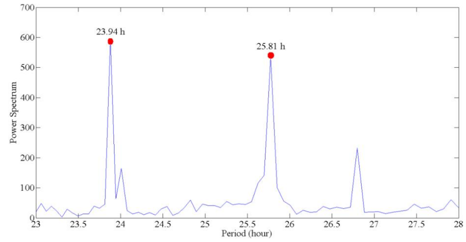

Figure 14. Power spectrum obtained from Fourier transform - diurnal components.

The power spectrum of the Workington tidal data has been also computed using the method of Fourier Transform. Similar time spans are used in every figure in order to compare this spectrum to the power spectrum computed by the LS-HE method. Figure 12 to Fig. 15 show the obtained results. The horizontal and vertical axes in these figures are as before.

The corresponding short period components are shown in Fig. 12. Figure 8 should be used in order to compare the power spectrum proposed by the LS-HE with this result. It is seen in Fig. 12b that the maximum power spectrum for the existing short period constituents in these tidal records is a component with frequency 6.211 hours, see the bullet in Fig. 12b.

The semidiurnal and diurnal parts of the computed power spectrum are shown in Fig. 13 and Fig. 14 respectively. Similar to

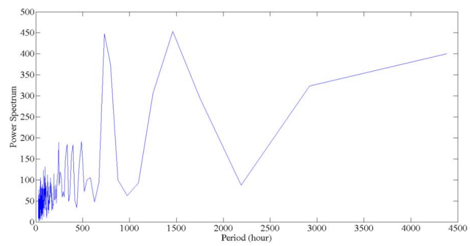

Figure 15. Power spectrum obtained from Fourier transform - long period components.

Fig. 12b, bullets are used in order to distinguish the tidal constituents with maximal power spectra from the others. Again, it is easily seen that these constituents are those that have been already approved by the LS-HE method (see Fig. 9 and Fig. 10).

The long period part of the computed power spectrum is shown in Fig. 15. As it can be seen, the power spectrums of these constituents are much smaller than the power spectrum of diurnal and semidiurnal components.

4. Conclusion

In this paper least squares harmonic estimation is used for analyzing the frequency content in both real tidal records and simulated time series. The applications of this method to simulated time series shows that the periodic constituents proposed by this method depend on two parameters: amplitudes of the frequencies and the data length. Components with small amplitudes cannot be detected through the hypothesis test of this method unless the length of the data record is sufficiently large. This is confirmed by the real tidal records.

Applications of this method to the tidal data in this research, results in constituents whose frequencies are close to the main tidal constituents have been already reported in the similar works which have been done others.

Although the LS-HE and Fourier power spectrums are not exactly the same, the power spectrum computed by the Fourier Transform includes the frequencies which have been detected by the least squares harmonic estimation technique. Moreover, the power spectra of these frequencies are also maximized in the Fourier method. This is an independent approach for validating the frequency content which is proposed by the least square harmonic estimation technique.

The LS-HE method can tolerate limited gaps in the data; it can also detect the main components in a periodic time series automatically. These two items are the main advantages of this method to the other existing techniques.

References

Abolghasem A. M., 1994, Determination of Sea Surface Topography along Persian Gulf, M.S thesis, K. N. Toosi University of Technology.

Agnew D.C., 2007, Earth Tides, Treatise on Geophysics: Geodesy, T. A. Herring, ed., Elsevier, New York, pp. 163-195.

Amiri-Simkooei A. R. and Asgari J., 2012, Harmonic analysis of total electron contents time series: methodology and results, GPS Solut, 16, 1, 77-88.

Amiri-Simkooei A. R., 2007, Least-squares variance component estimation: Theory and GPS applications, Ph.D. thesis, Delft University of Technology, Publication on Geodesy, 64, Netherlands Geodetic Commission, Delft.

Amiri-Simkooei A. R., Tiberius C. C. J. M. and Teunissen P. J. G., 2007, Assessment of noise in GPS coordinate time series: methodology and results, J. Geophys. Res., 112, B07413.

Amiri-Simkooei A. R. and Tiberius C. C. J. M., 2007, Assessing receiver noise using GPS short baseline time series, GPS Solut, 11, 1, 21-35.

Cartwright D. E. and Tayler R. J., 1971, New computations of the tide-generating potential, Ceophys. J. R. astr. SOC., 23, 45–74.

Darwin G. H., 1907, The Scientific Papers of Sir George Darwin, Oceanic Tides and Lunar Disturbance of Gravity, Cambridge University Press.

Doodson A. T., 1921, The harmonic development of the tide generating potential, Proceedings of the Royal Society Series A 100: 305–329.

Epler J., 2010, Tidal Resource Characterization from Acoustic Doppler Current Profilers, University of Washington, Department of Mechanical Engineering.

Foreman M. G. G., 1977, Manual For Tidal Heights Analysis and Prediction, Pacific Marine Science Report, 77,10.

Ghil M. and Taricco C., 1997, Advanced spectral analysis methods, in: Past and Present Variability of the Solar-terrestrial System: Measurement, Data Analysis and Theoretical Models, 137–159.

House M. R., 1995, Orbital forcing timescales: an introduction, Geological Society, London, Special Publications, 85, 1-18.

Hartmann T. and Wenzel H.G., 1995, The HW95 tidal potential catalogue. Geophys. Res. Lett, 22, 3553–3556.

Kudryavtsev S. M., 2004, Improved harmonic development of the Earth tide-generating potential, J. Geod., 77, 829–838.

Teunissen P. J. G., 2000a, Adjustment theory: an introduction. Website http://www.vssd.nl: Delft University Press. Series on Mathematical Geodesy and Positioning.

Teunissen P. J. G., Simons D. G. and Tiberius C. C. J. M. ,2005, Probability and observation theory, Faculty of Aerospace Engineering, Delft University of Technology: Delft University. Lecturenotes AE2-E01.

Vanicek P., 1969, Approximate spectral analysis by least-squares fit. Astrophys. Space Sci., 4, 387–391.

Vanicek P. and Krakiwsky E.J., 1986, Geodesy: The Concepts, Elsevier Science publisher, ISBN:0-444-87775-4.

Wahr J., 1995,Earth Tides, Global Earth Physics, A Handbook of Physical Constants, AGU Reference Shelf, 1, 40-46.

Appendix A:

Computed amplitudes of the tidal constituents proposed in Foreman (1977) at Workington and Bandar Abbas stations using least-squares estimation technique.

No.	Constituent's name	Frequency	Period (hour)	Amplitude in Workington	Amplitude in BandarAbbas
1	S_a	0.00011407	8766.5469	0.21146298	0.1057027
2	S_{sa}	0.00022816	4382.8892	0.13544653	0.0342881
3	M_{sm}	0.00130978	763.487	0.09548087	0.0103083
4	M_m	0.00151215	661.31006	0.04908334	0.0042576
5	M_{sf}	0.00282193	354.3674	0.02543426	0.0104729
6	M_f	0.00305009	327.85918	0.04803538	0.005116
7	α_1	0.03439657	29.072666	0.007182	0.0032008
8	$2Q_1$	0.03570635	28.006223	0.0155372	0.0068264
9	σ_1	0.03590872	27.848389	0.00844063	0.0134962
10	Q_1	0.0372185	26.868358	0.05379317	0.0455956
11	ρ_1	0.03742087	26.723056	0.00811684	0.0032334
12	O_1	0.03873065	25.819345	0.13426803	0.2184626
13	τ_1	0.03895881	25.668135	0.00910208	0.0045188
14	β_1	0.04004043	24.974757	0.00139518	0.0028009
15	NO_1	0.04026859	24.833251	0.00702346	0.013728
16	ξ_1	0.04047097	24.709069	0.00914395	0.0037149
17	π_1	0.04143851	24.132142	0.00062021	0.0076051
18	P_1	0.04155259	24.065889	0.04194575	0.1111651
19	S_1	0.04166667	23.999998	0.01214004	0.0131236
20	K_1	0.04178075	23.934467	0.13616127	0.3434935
21	PSI_1	0.04189482	23.869299	0.00756443	0.0082615
22	ϕ_1	0.04200891	23.804474	0.00933087	0.0049311
23	THE_1	0.04309053	23.206955	0.00737446	0.0099052
24	J_1	0.0432929	23.098476	0.0112118	0.0198399
25	SO_1	0.04460268	22.420177	0.00979142	0.0068162
26	OO_1	0.04483084	22.306073	0.00165179	0.0092185
27	UPS_1	0.04634299	21.578237	0.00504431	0.0025932
28	OQ_2	0.07597494	13.162235	0.01660253	0.0187536
29	ε_2	0.07617731	13.127268	0.00684685	0.0100495
30	$2N_2$	0.0774871	12.905374	0.0820264	0.0423768
31	μ_2	0.07768947	12.871757	0.01519657	0.0131031
32	N_2	0.07899925	12.658348	0.51128783	0.2760667
33	ν_2	0.07920162	12.626004	0.1142547	0.0397039
34	γ_2	0.08030903	12.4519	0.01673032	0.0199884
35	H_1	0.08039733	12.438224	0.01253026	0.0327271
36	M_2	0.0805114	12.420601	2.65376192	1.0974962
37	H_2	0.08062547	12.403028	0.01090011	0.0158088
38	MKS_2	0.08073957	12.385501	0.00797598	0.0077313
39	λ_2	0.08182118	12.221774	0.05548108	0.0282808
40	L_2	0.08202355	12.191621	0.12785633	0.0647393
41	T_2	0.08321926	12.016449	0.04758102	0.0283308
42	S_2	0.08333334	11.999999	0.8888338	0.4250608
43	R_2	0.0834474	11.983597	0.01582706	0.0040119
44	K_2	0.08356149	11.967235	0.33310515	0.1114423
45	MSN_2	0.08484548	11.786132	0.03140672	0.0040964
46	η_2	0.08507364	11.754522	0.00929708	0.0101787
47	MO_3	0.11924206	8.3863026	0.00884573	0.0203557
48	M_3	0.1207671	8.2804009	0.01671408	0.0227847
49	SO_3	0.12206399	8.1924243	0.00679491	0.0152056
50	MK_3	0.12229215	8.1771397	0.00944616	0.0265216
51	SK_3	0.12511408	7.9927055	0.0081406	0.0182745
52	MN_4	0.15951064	6.2691743	0.05136069	0.0139801
53	M_4	0.1610228	6.2103007	0.12872517	0.0209033
54	SN_4	0.16233259	6.1601925	0.00968357	0.0027687
55	MS_4	0.16384473	6.1033394	0.06779774	0.0067447
56	MK_4	0.1640729	6.0948517	0.02683817	0.0031409
57	S_4	0.16666667	5.9999999	0.00810351	0.0016646
58	SK_4	0.16689482	5.9917977	0.00672517	0.0055354
59	$2MK_5$	0.20280355	4.9308802	0.00187223	0.0027925
60	$2SK_5$	0.20844743	4.7973727	0.00028105	0.0011006
61	$2MN_6$	0.24002205	4.1662839	0.00621312	0.0027239
62	M_6	0.2415342	4.1402004	0.01336912	0.0029541
63	$2MS_6$	0.24435613	4.0923876	0.01754958	0.0043935
64	$2MK_6$	0.24458429	4.08857	0.0067727	0.0037387
65	$2SM_6$	0.24717808	4.0456662	0.00458662	0.003279
66	MSK_6	0.24740623	4.0419354	0.00319784	0.0024747
67	$3MK_7$	0.28331494	3.5296409	0.00050051	0.0007464
68	M_8	0.32204559	3.1051504	0.00230324	0.0007153